Supplement of Hydrol. Earth Syst. Sci., 21, 5823–5846, 2017
https://doi.org/10.5194/hess-21-5823-2017-supplement

Hydrology and Earth System Sciences
Open Access

Supplement of

Simple scaling of extreme precipitation in North America

Silvia Innocenti et al.

Correspondence to: Silvia Innocenti (silvia.innocenti@ete.inrs.ca)

Introduction

This supporting information presents some extended results and describes in more details some methodological developments. It is structured as follows. Table S1 lists in alphabetic order the recurrent acronyms used in text. Figure S1 displays the station locations and the median of the distribution of the annual maximum precipitation for various durations considered in the study. Figures S2 and S3 show results for the SS model validation (Slope and GOF tests) when AMS are pooled according to the instrument and temporal resolution. Section S1 briefly describes these figures. Figure S4 presents the results of the cross-validation experiment for the SS model (Slope and GOF tests) for each duration and scaling interval. Figures S5 and S6 present, respectively, the regional distribution of the mean number of events per year, $\bar{N}_{eve}$, and the mean wet time, $\bar{T}_{wet}$, of these events for each 6-duration scaling interval. The detailed definition of $\bar{N}_{eve}$ and $\bar{T}_{wet}$ is given in Sect. S2. Finally, Fig. S9 to S17, extend to longer scaling intervals the analysis presented in Sect. 4.3 (Regional analysis) and Sect. 5.2 (SS-GEV model evaluation) for 6-duration scaling intervals.

Section S1: Details on Fig. S2 and S3 .

Figures S2 and S3 show the results of the Slope and GOF tests applied at the 0.05 significance level when AMS are pooled according to the instrument and temporal resolution of the recording station. Each of the 12 matrices of these figures represents the proportion of valid SS stations [see the definition of valid SS station in Sect. 4.1 and in Fig. 1 (e) of the paper] for each duration (vertical axis) and scaling intervals (horizontal axis).

Each grid-box of the heatmaps is divided in two triangles. Upper triangles in Fig. S2 correspond to the fraction of AMS having instrument resolution $< 2.54\ \mathrm{mm}$, while lower triangles correspond to AMS with instrument resolution of $2.54\ \mathrm{mm}$. Tip resolution at each station is defined as the minimum non-zero recorded value. Tip resolution at stations having both DPDM and HCPD series, or both 15PD and HPD series, was defined as the maximum value between the resolutions of these two series.

Upper triangles in Fig. S3 correspond to the fraction of AMS constructed from both HPD and 15PD series, or both HCPD and DMPD series (i.e. with temporal resolution $\leq 1\ \mathrm{h}$). Lower triangles correspond to the fraction of AMS estimated from hourly series only (series constructed from HCPD or HPD series, i.e. a $1\mathrm{h}$ temporal resolution).

White triangles in Fig. S2 and S3 indicate non-significant differences between upper and lower triangle proportions. Tests on proportion differences were applied at significance level 0.05 without accounting for the spatial autocorrelation among stations.

Section S2: Definition of $\bar{N}_{eve}$ and $\bar{T}_{wet}$ for the events sampled within each scaling interval

To provide deeper insights about regional features of precipitation associated with specific scaling regimes, two variables related to the precipitation events observed within AMS were also analyzed: the mean number of events per year, $\bar{N}_{eve}$, and the mean wet time per event, $\bar{T}_{wet}$, contributing to AMS within each scaling interval.

For a given year and station, annual maxima associated to different durations of a given scaling interval were considered to belong to the same precipitation event if the time intervals over which they occurred overlapped [see Fig. S5 (g); in this example 3, 4, and 5 h annual maxima are associated with the first event while 1, 2, and 6 h annual maxima are associated to the second event]. The mean number of events at each station was then computed:

$$\bar{N}_{eve} = \frac{1}{n}\sum_{i}^{n} N_{eve,i} \tag{1}$$

with $N_{eve,i}$ the number of non-overlapping time intervals, i.e. the number of different events contributing to AMS during the i^{th} year of record. The distribution of $\bar{N}_{eve}$ values within each region is presented in Fig. S5.

For each station, the mean wet time, $\bar{T}_{wet}$ $[hours]$, of events sampled within each scaling interval was computed as:

$$\bar{T}_{wet} = n_E^{-1}\sum_{e}^{n_E} T_{wet,e} \tag{S2}$$

with n_E the total number of events e sampled by the annual maxima precipitation series in the scaling interval [see Sect. 4.3 of the article for the definition of each event]. $T_{wet,e}$ is the wet time of the e^{th} event:

$$T_{wet,e} = W_e T_e \tag{S2}$$

where W_e is the fraction of event time steps during which positive precipitation depths were recorded, and T_e is the total event duration (in hours).

Figure S6 displays the distribution over valid SS stations of $\bar{T}_{wet}$ within each region [Fig. S6 (a) to (f)] and one example of calculation of $T_{wet,e}$ and $\bar{T}_{wet}$ [Fig. S6 (g)].

Table 1. List of the relevant acronyms recurring in the manuscript.

AD:	Anderson Darling *test*	**KS:**	Kolmogorov-Smirnov *test*
AMS:	Annual Maxima Series	**ML:**	Maximum-Likelihood *estimation*
GEV:	Generalized Extreme Value *distribution*	**MS:**	Multiscaling
GOF:	Goodness-Of-Fit *test*	**MSA:**	Moment Scaling Analysis
IQR:	Interquartile Range	**PWM:**	Probability Weighted Moments *estimation*
IDF:	Intensity-Duration-Frequency *curve*	**SS:**	Simple Scaling

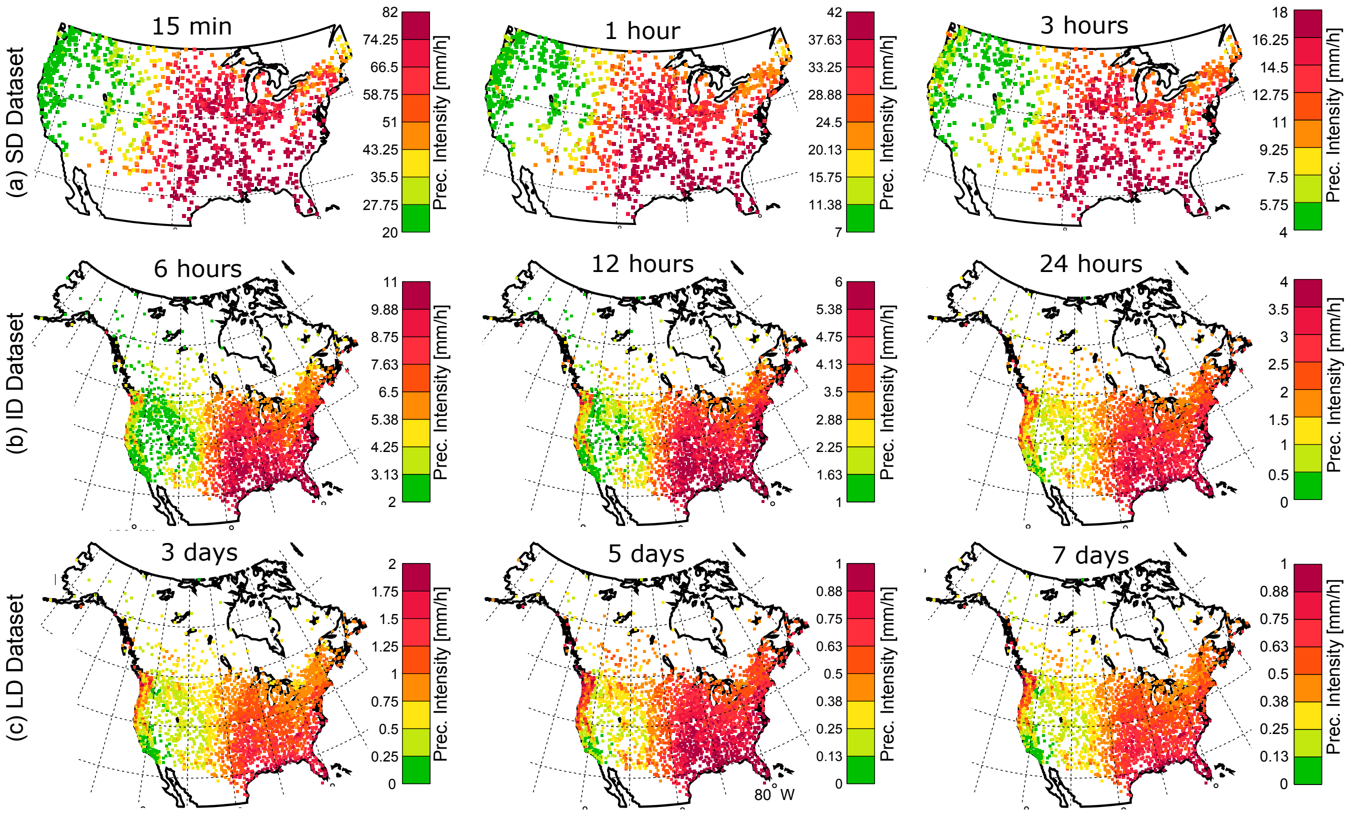

Figure S1. Spatial distribution of the median precipitation intensity for: (a) 15 min, 1 h, and 3 h in the SD dataset, (b) 6 h, 12 h, and 24 h in the ID dataset, and (c) $3days$, $5days$, and $7days$ in the LD datasets.

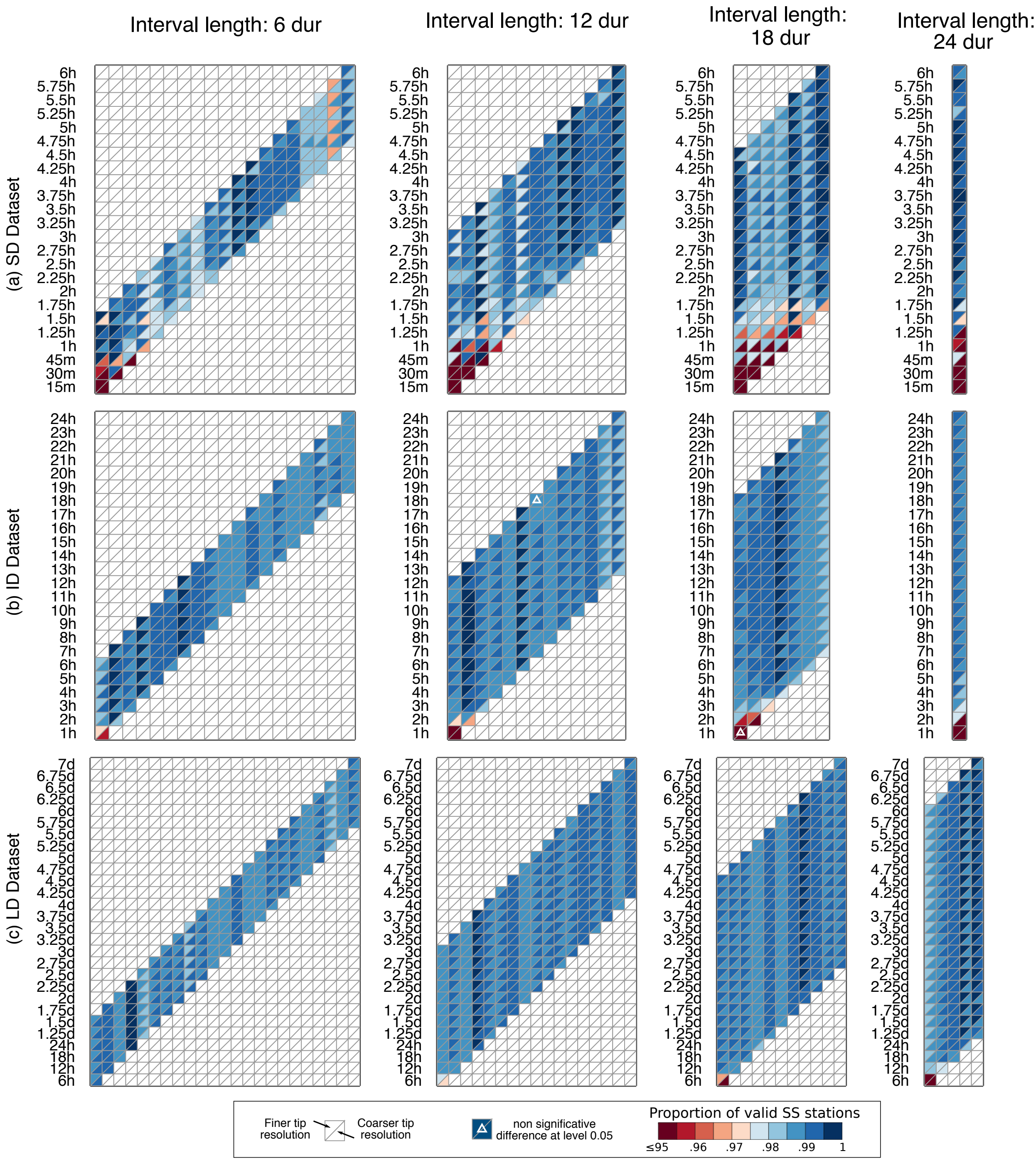

Figure S2. Proportion of valid SS stations for each duration and scaling interval for the SD, ID, and LD datasets [row (a), (b), and (c) respectively] when accounting for series instrument resolutions. Upper triangles correspond to the fraction of AMS having instrument resolution < 2.54 mm, while lower triangles correspond to AMS with instrument resolution of 2.54 mm. White triangles indicate non-significant differences between upper and lower triangle proportions. See Sect. S1 for details.

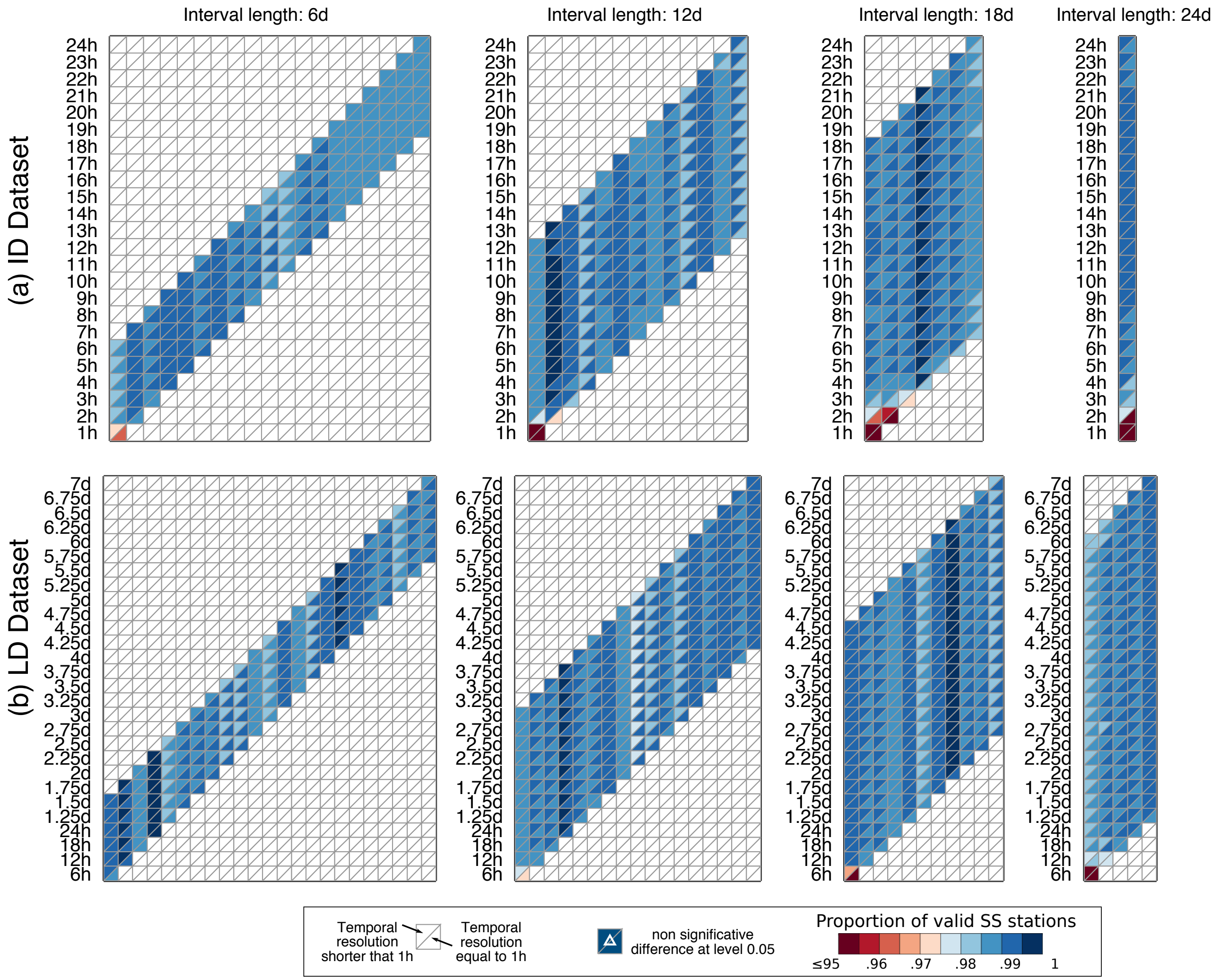

Figure S3. Proportion of valid SS stations for each duration and scaling interval for (a) ID and (b) LD datasets when accounting for series temporal resolutions Upper triangles in Figures S3 correspond to the fraction of AMS with temporal resolution ≤ 1 h. Lower triangles correspond to the fraction of AMS estimated from hourly series only. White triangles indicate non-significant differences between upper and lower triangle proportions. See Sect. S1 for details.

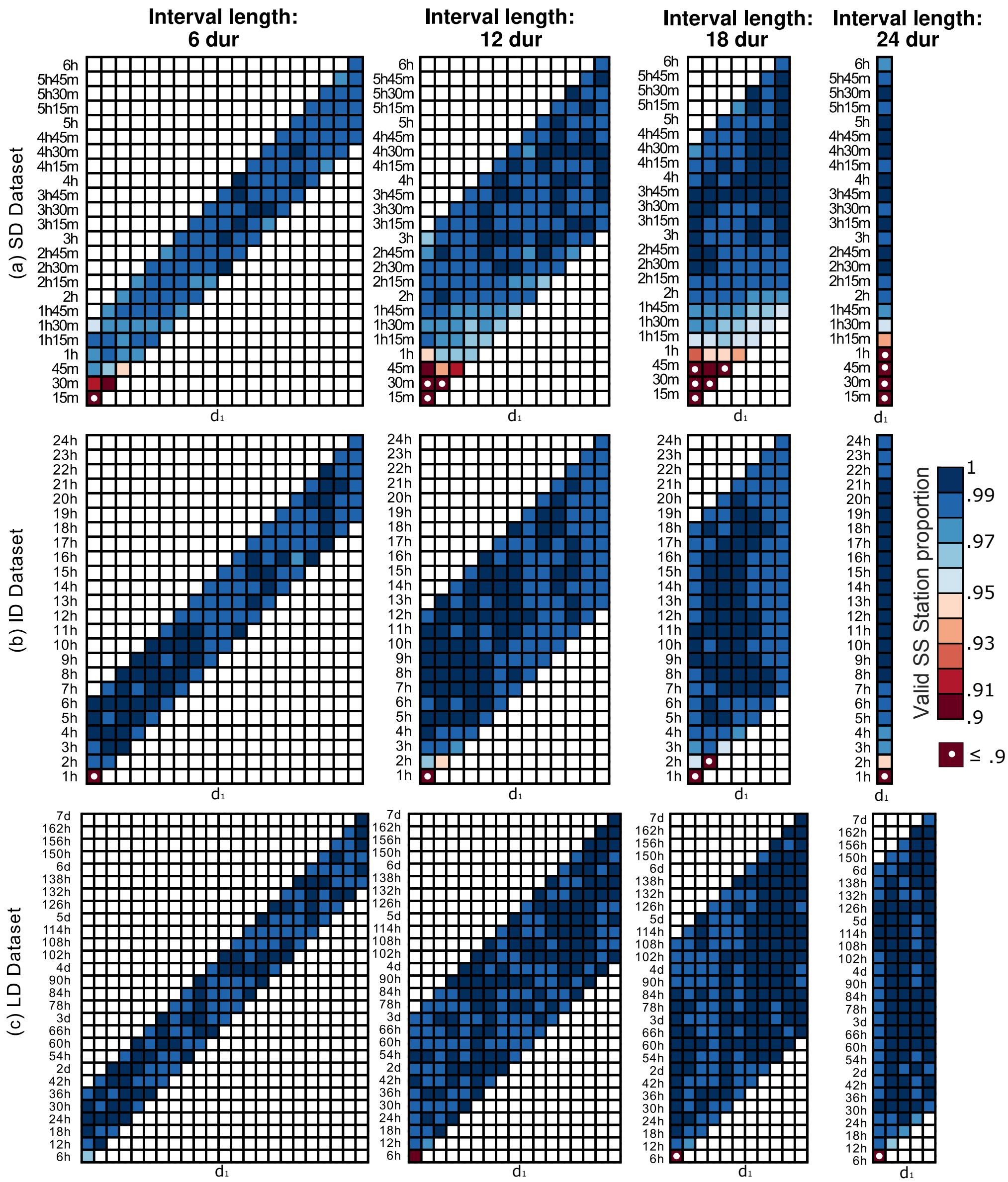

Figure S4. Proportion of stations satisfying both the Slope and GOF tests applied at the 0.95 confidence level in cross-validation. Each grid-box represents the proportion for a duration (vertical axis) and scaling interval (horizontal axis) for the SD, ID, and LD datasets [row a), b), and c) respectively] computed when that duration is excluded from the scaling interval. White circles indicate proportions lower than 0.90.

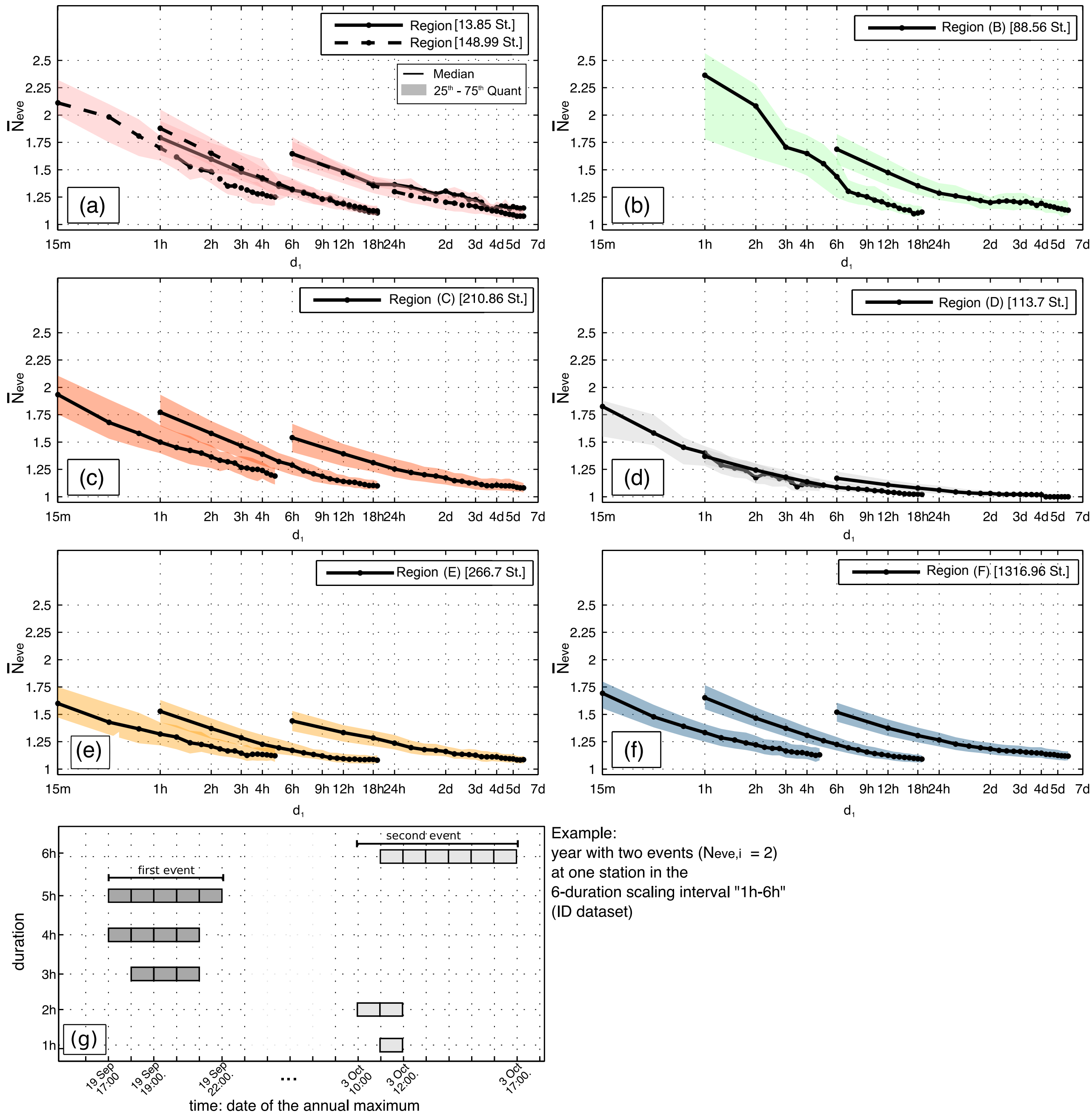

Figure S5. Median and Interquantile Range (IR) of the distribution over valid SS stations of the mean number of events per year, $\bar{N}_{eve}$, within each region of Fig. 7 for each 6-duration scaling interval for the SD (left curve), ID (central curve), and LD (right curve) datasets. For each region, the mean number of valid SS stations over the scaling intervals is indicated in the legend in brackets. Panel (g) displays an example of how $N_{eve,i}$ is estimated for year i.

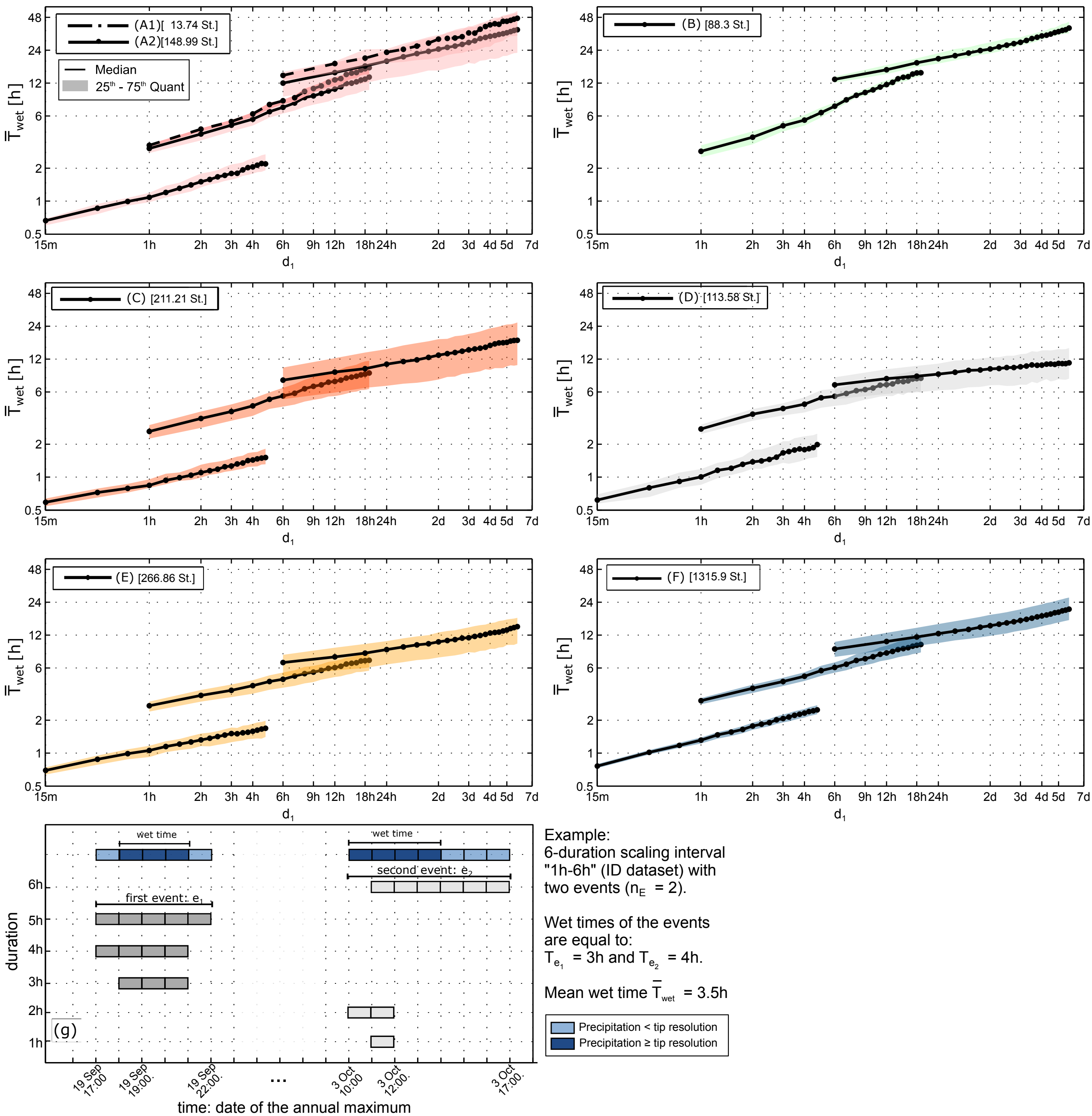

Figure S6. Median and Interquantile Range (IR) of the distribution over valid SS stations of the mean wet time, $\bar{T}_{wet}$, within each region for each 6-duration scaling interval in the SD (left curve), ID (central curve), and LD (right curve) datasets. Graph (g) displays an example of how $\bar{T}_{wet}$ is estimated for one theoretical scaling interval. For each region, the mean number of valid SS stations over the scaling intervals is indicated in brackets.

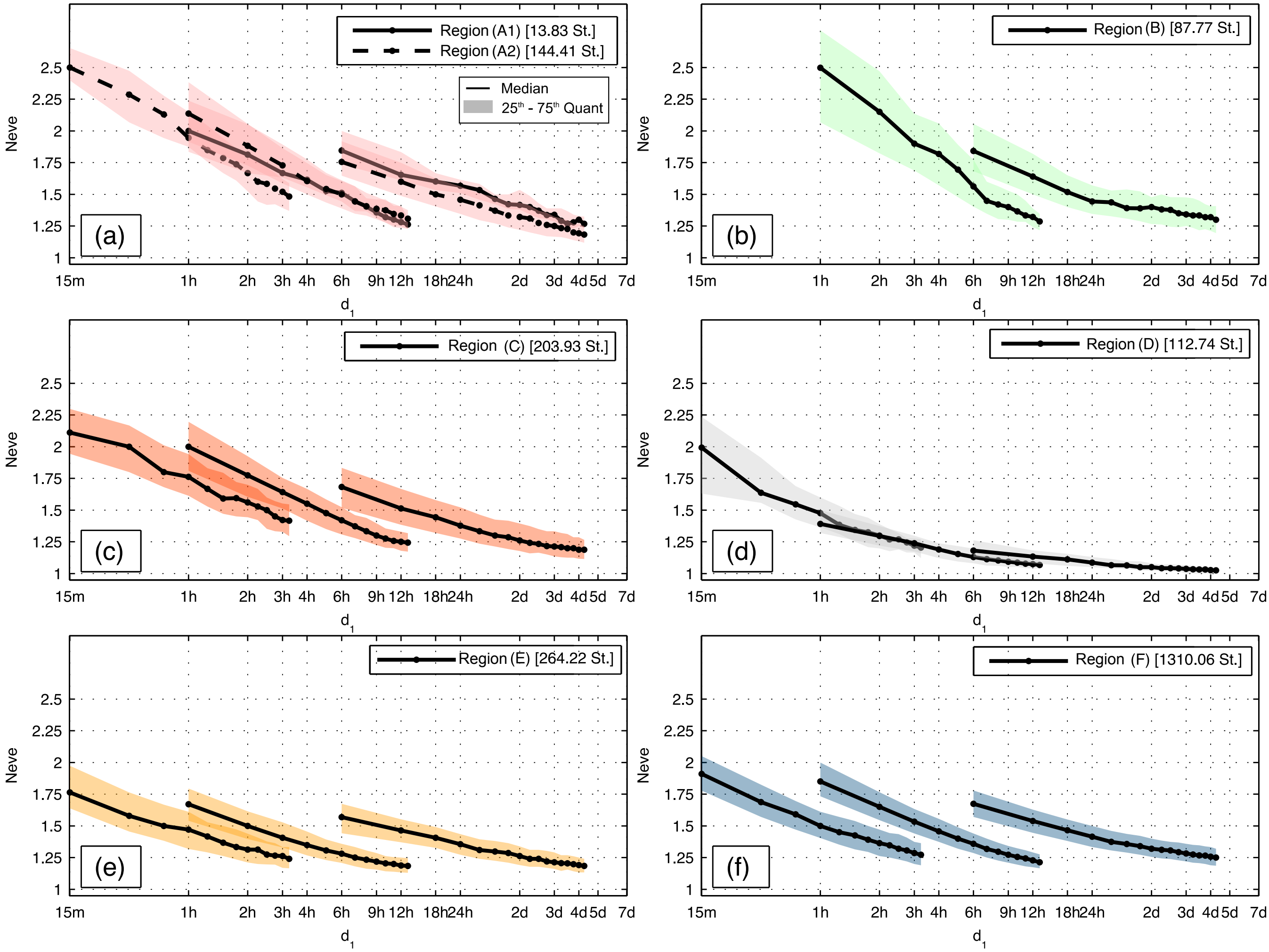

Figure S7. Median and Interquantile Range (IR) of the distribution over valid SS stations of the mean number of events per year, $\bar{N}_{eve}$, within each region for each 12-duration scaling interval for the SD (left curve), ID (central curve), and LD (right curve) datasets. For each region, the mean number of valid SS stations over the scaling intervals is indicated in brackets.

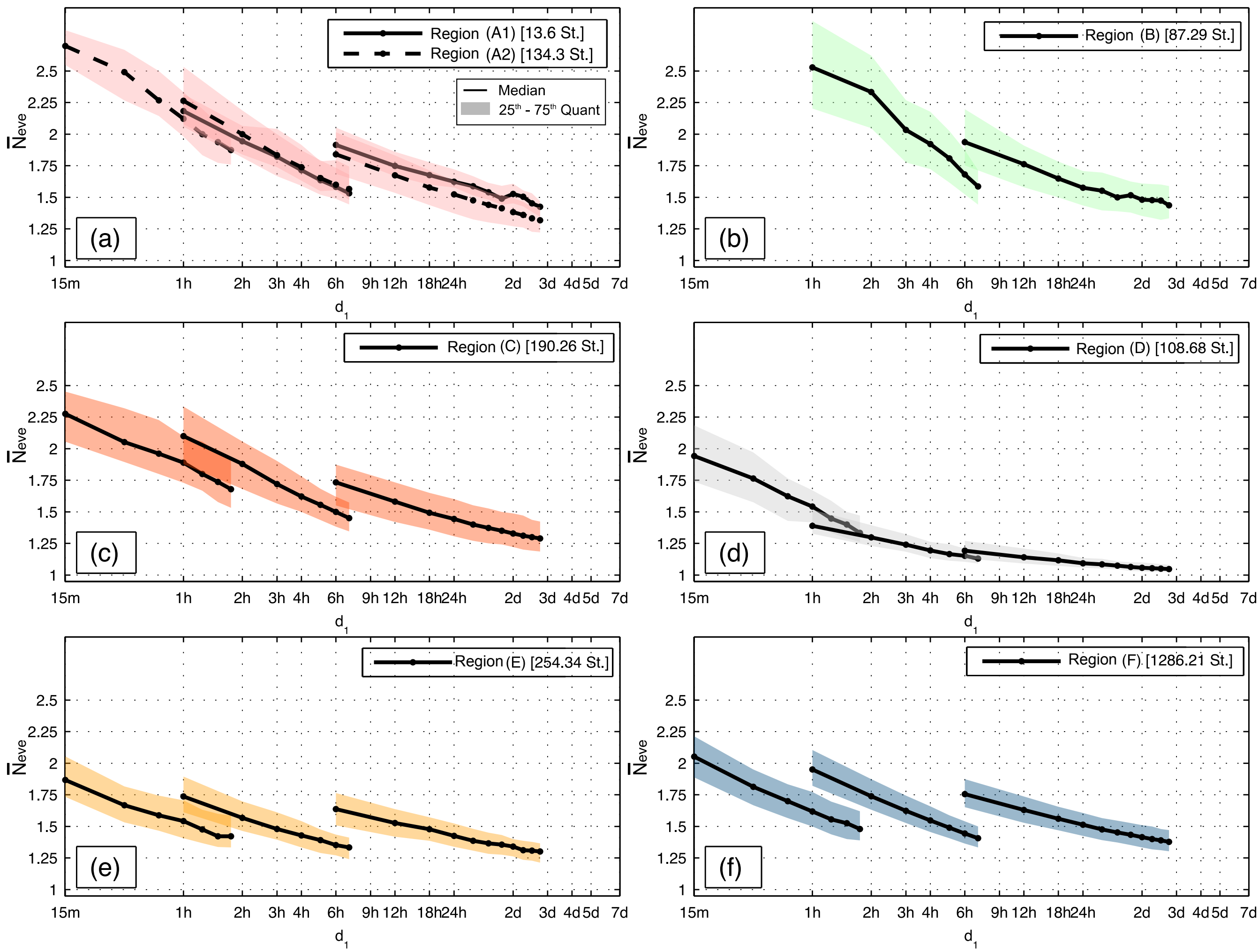

Figure S8. Median and Interquantile Range (IR) of the distribution over valid SS stations of the mean number of events per year, $\bar{N}_{eve}$, within each region for each 18-duration scaling interval for the SD (left curve), ID (central curve), and LD (right curve) datasets. For each region, the mean number of valid SS stations over the scaling intervals is indicated in brackets.

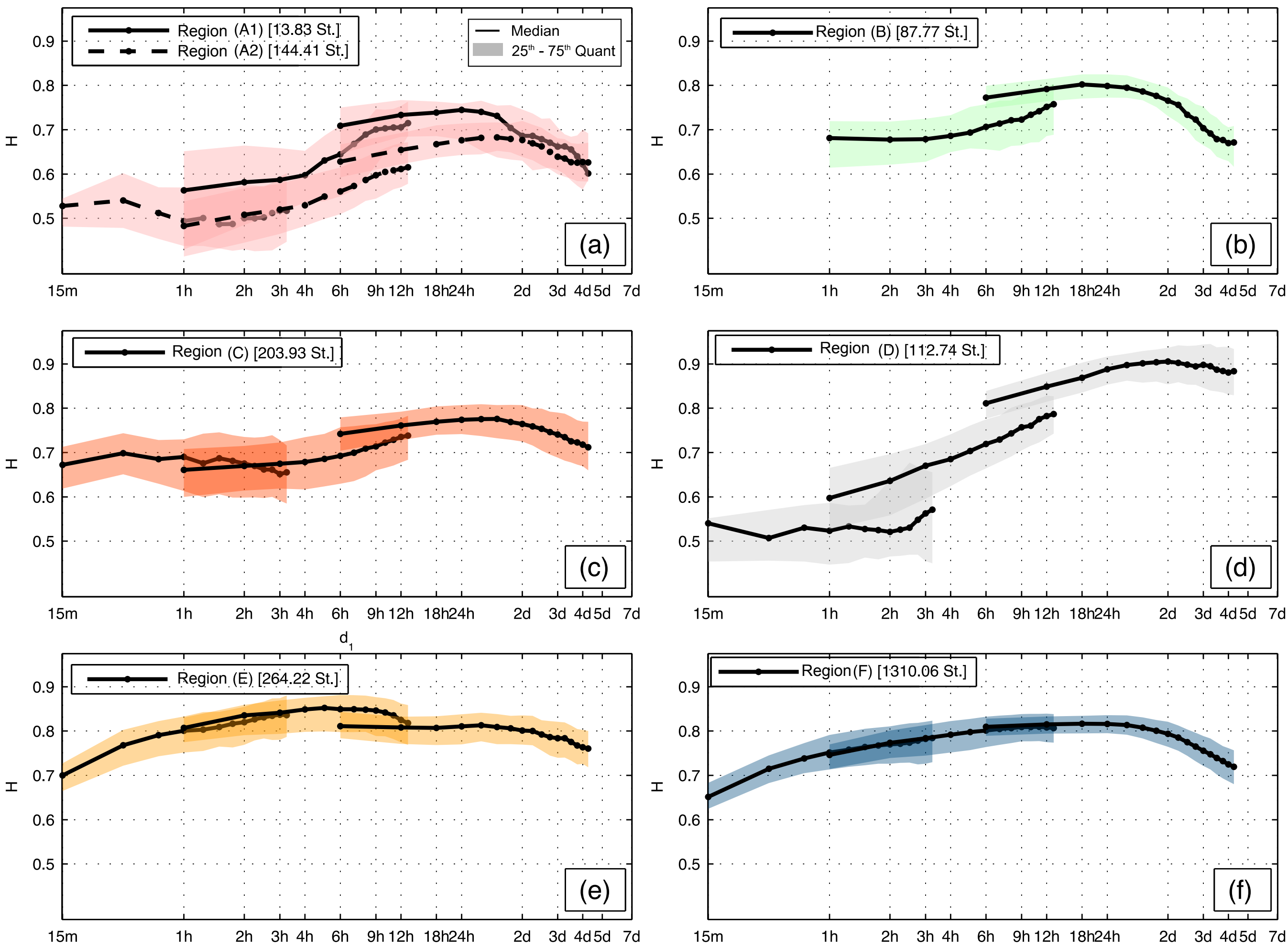

Figure S9. Median and Interquantile Range (IR) of the scaling exponent distribution over valid SS stations within each region for 12-duration scaling intervals in the SD (left curve), ID (central curve), and LD (right curve) datasets. For each region, the mean number of valid SS stations over the scaling intervals is indicated in brackets.

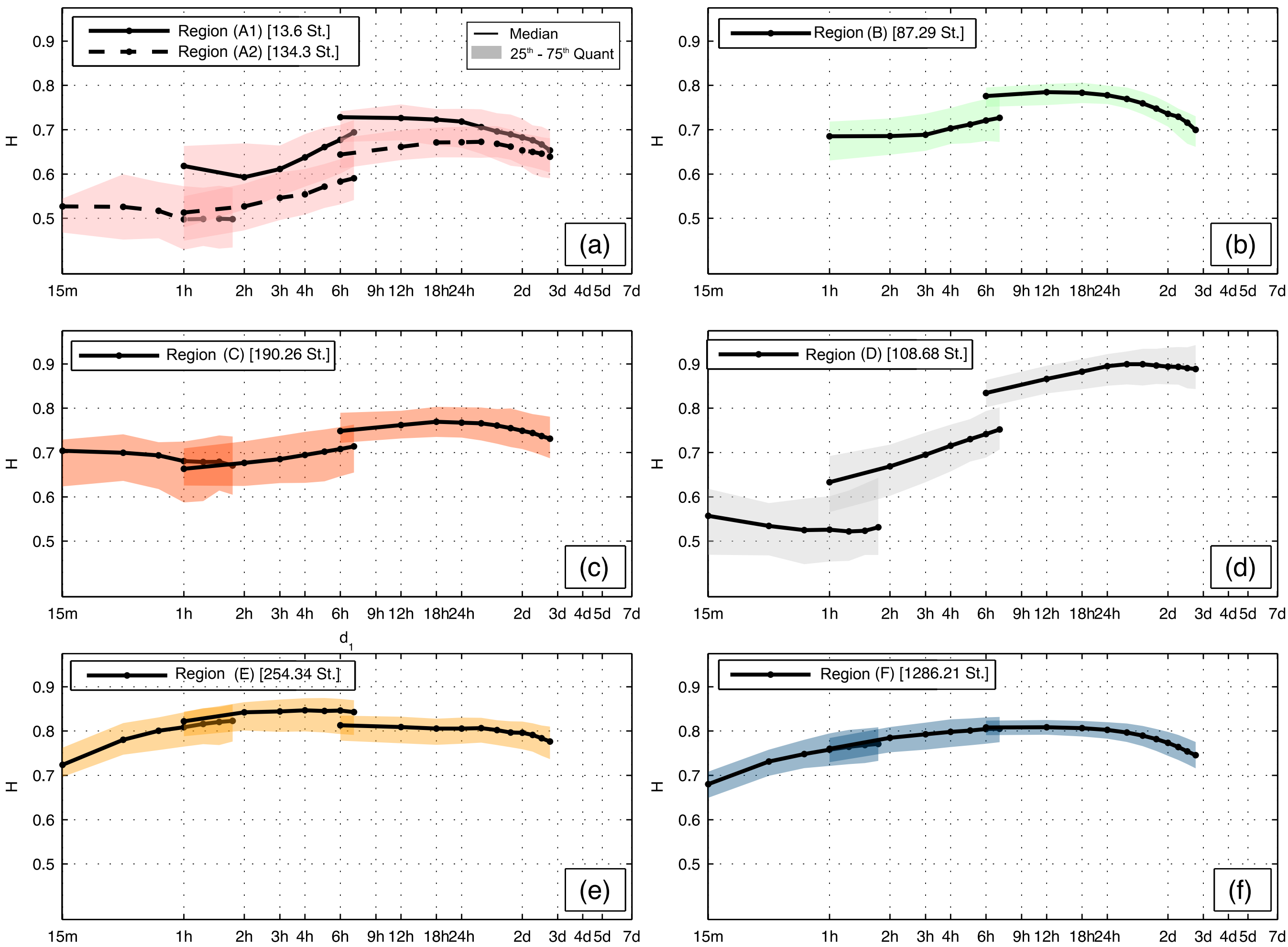

Figure S10. Median and Interquantile Range (IR) of the scaling exponent distribution over valid SS stations within each region for 18-duration scaling intervals for the SD (left curve), ID (central curve), and LD (right curve) datasets. For each region, the mean number of valid SS stations over the scaling intervals is indicated in brackets.

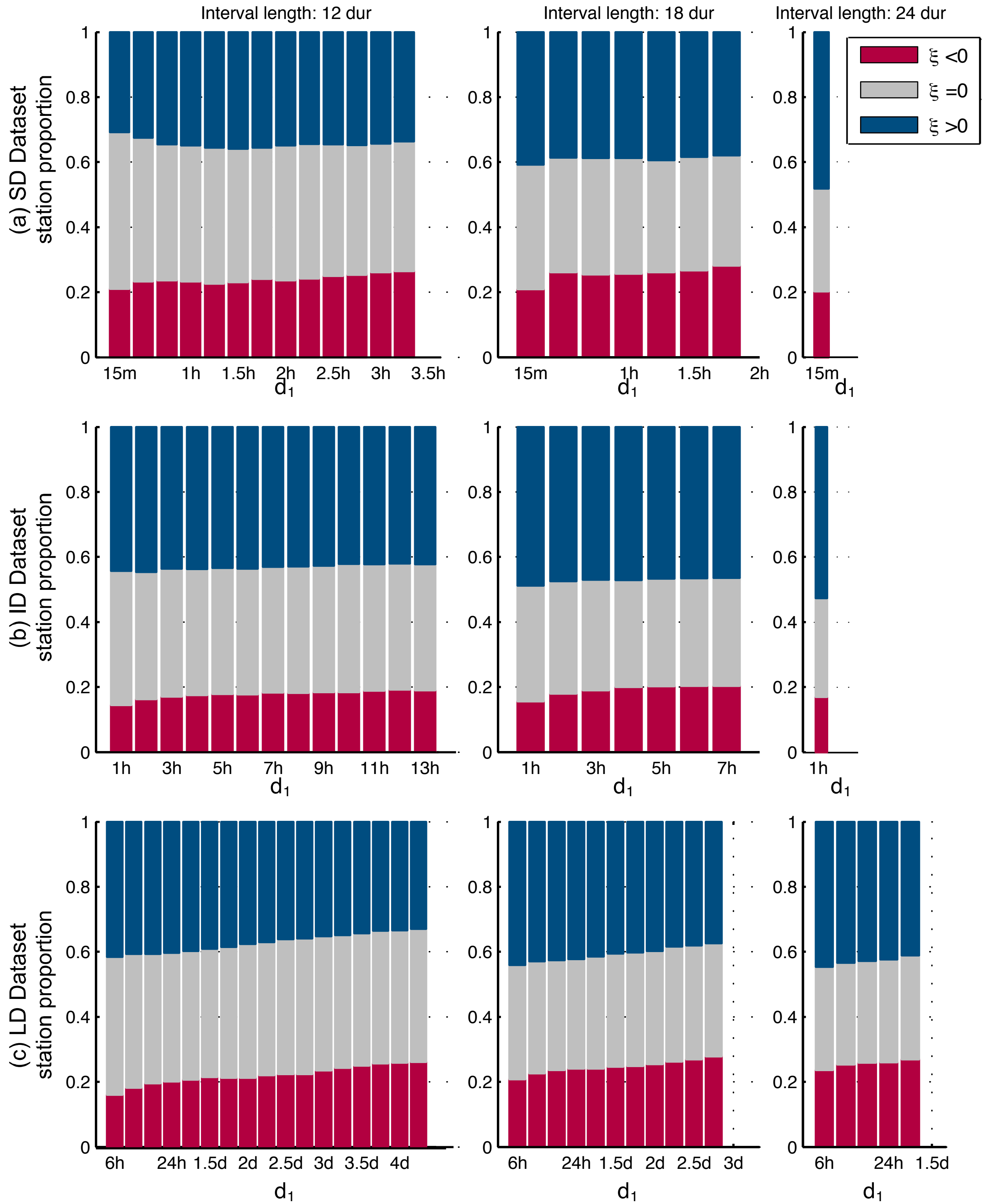

Figure S11. Stacked proportion of valid SS stations with $\xi < 0$ (in red), $\xi = 0$ (in grey), and $\xi > 0$ (in blue) for each 12-, 18-, and 24-duration scaling interval [1^{st}, 2^{nd}, and 3^{rd} col., respectively] in SD, ID, and LD datasets [(a), (b), and (c), respectively] .

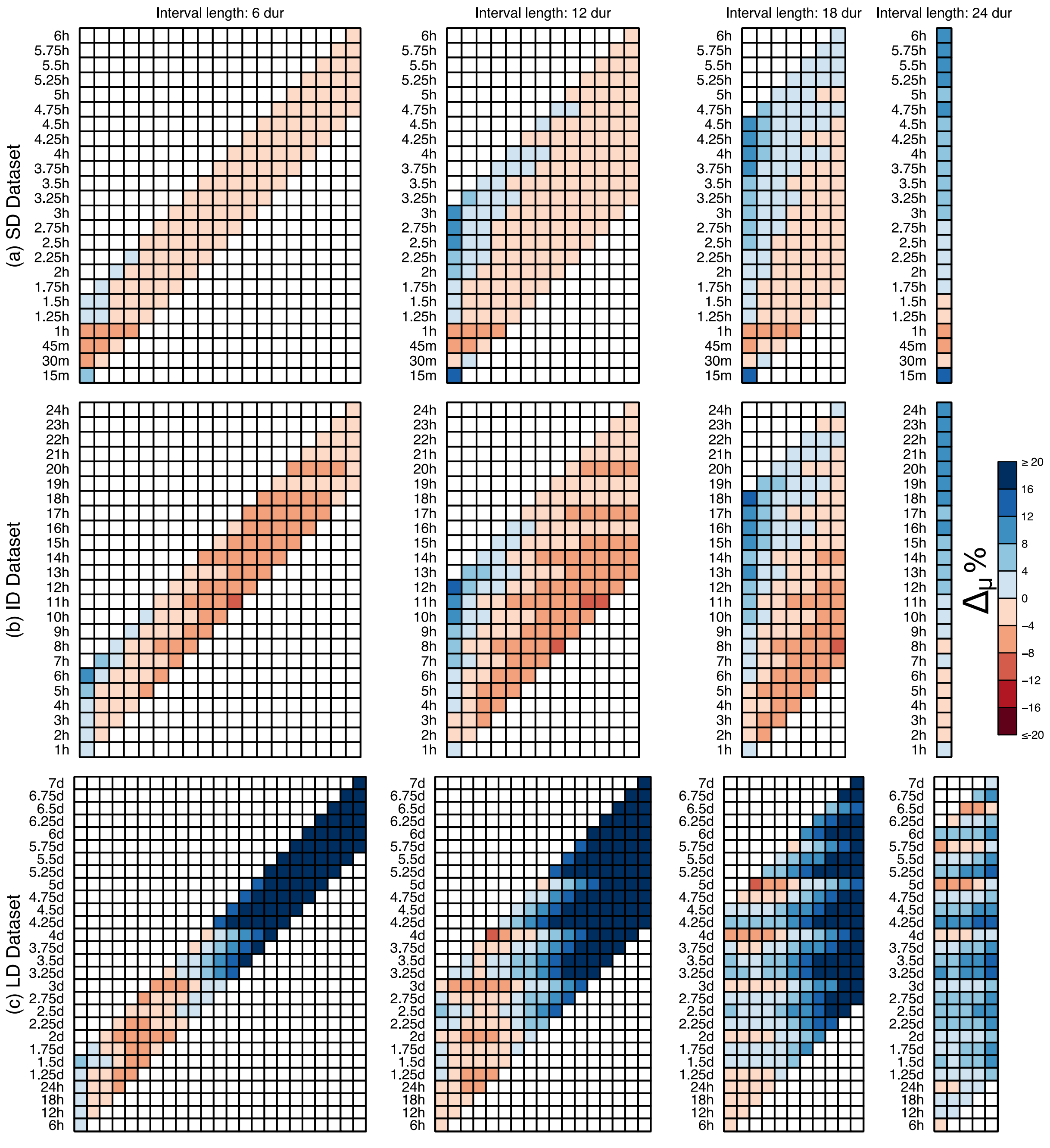

Figure S12. Median relative difference Δ_μ for each for each scaling interval (horizontal axis) and duration (vertical axis) in SD, ID, and LD datasets [(a), (b), and (c), respectively] .

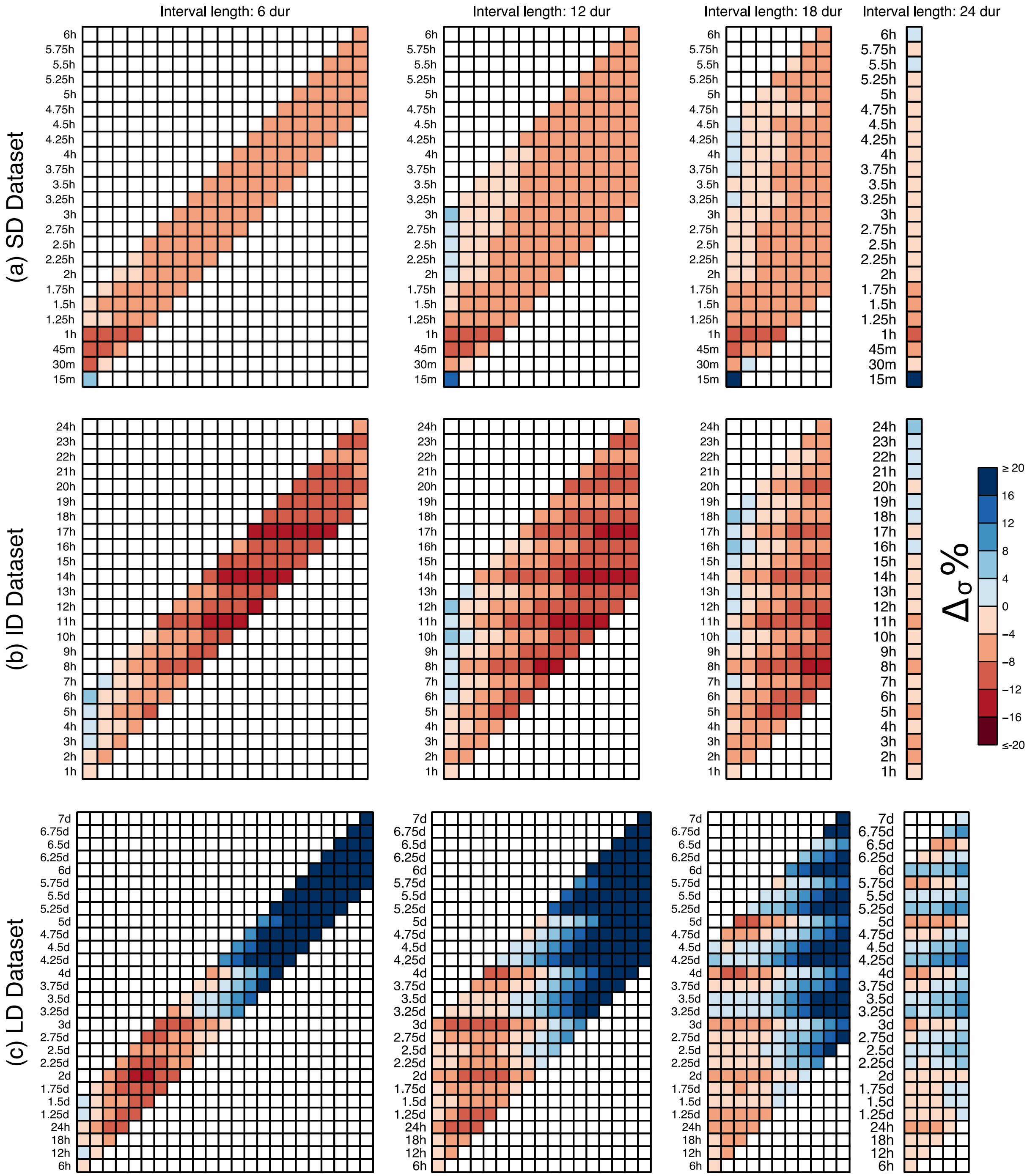

Figure S13. Median relative difference Δ_σ for each scaling interval (horizontal axis) and duration (vertical axis) in SD, ID, and LD datasets [(a), (b), and (c), respectively] .

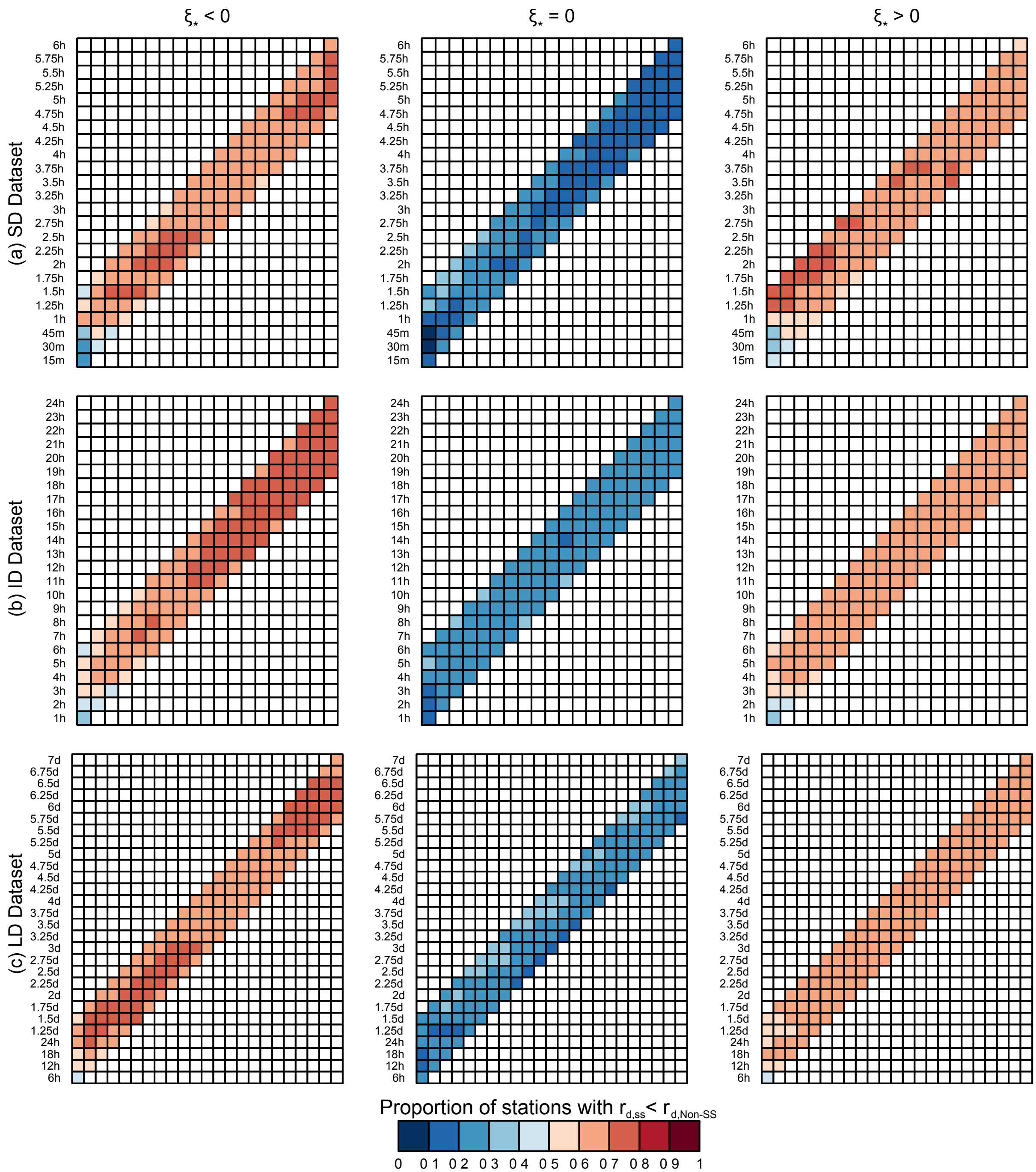

Figure S14. Proportion of valid SS stations having $r_{d,ss} < r_{d,non-SS}$ for $\xi_* < 0$ (1^st col.), $\xi_* = 0$ (2^nd col.), and $\xi_* > 0$ (3^rd col.) for each 6-duration scaling interval (horizontal axis) and duration (vertical axis) in SD, ID, and LD datasets [(a), (b), and (c), respectively] .

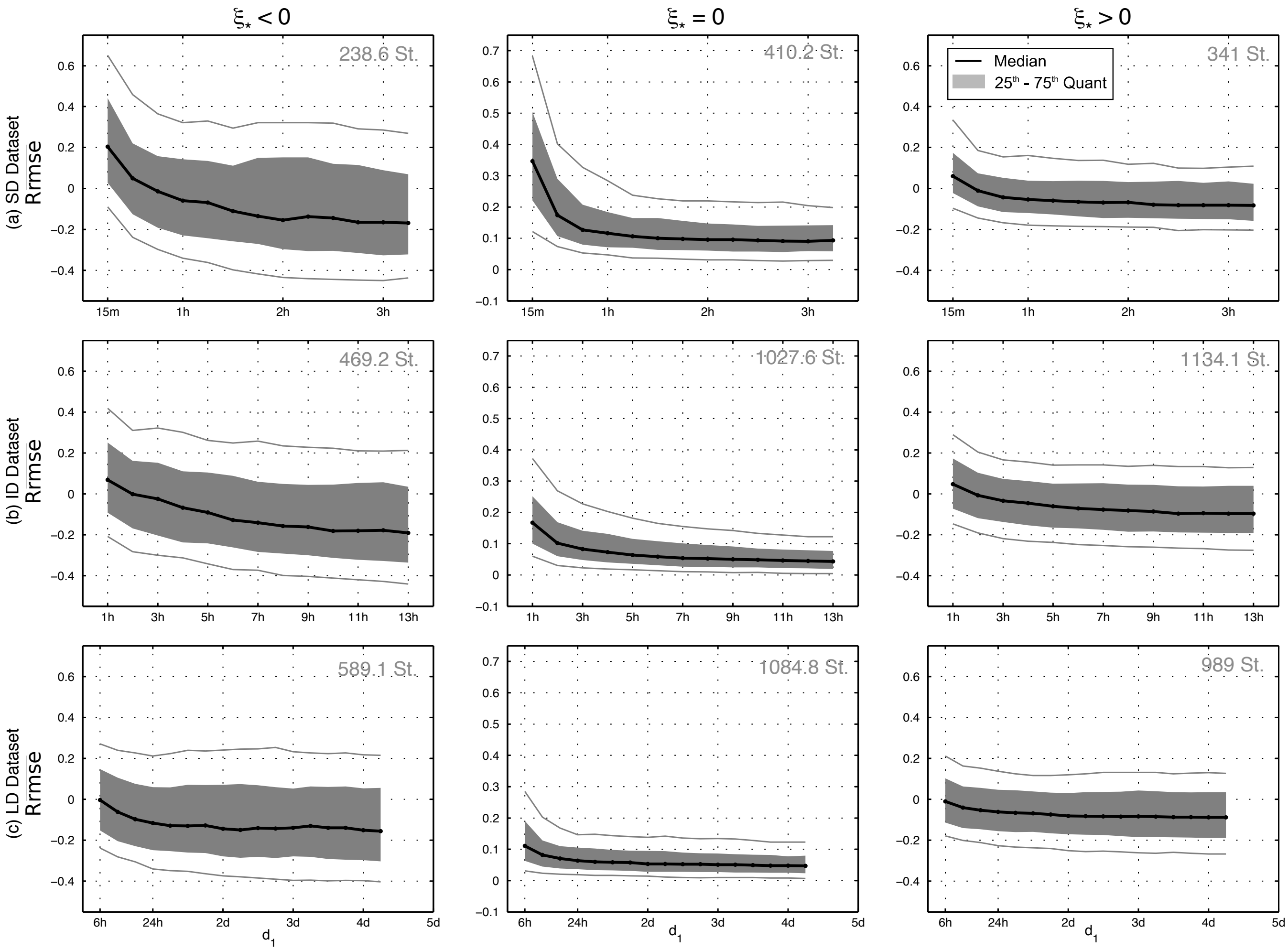

Figure S15. Distribution of the relative total RMSE ratio, $R_{\overline{rmse}}$, for $\xi_* < 0$ (1^st col.), $\xi_* = 0$ (2^nd col.), and $\xi_* > 0$ (3^st col.) for 12-duration scaling intervals in SD, ID, and LD datasets [(a), (b), and (c), respectively] .

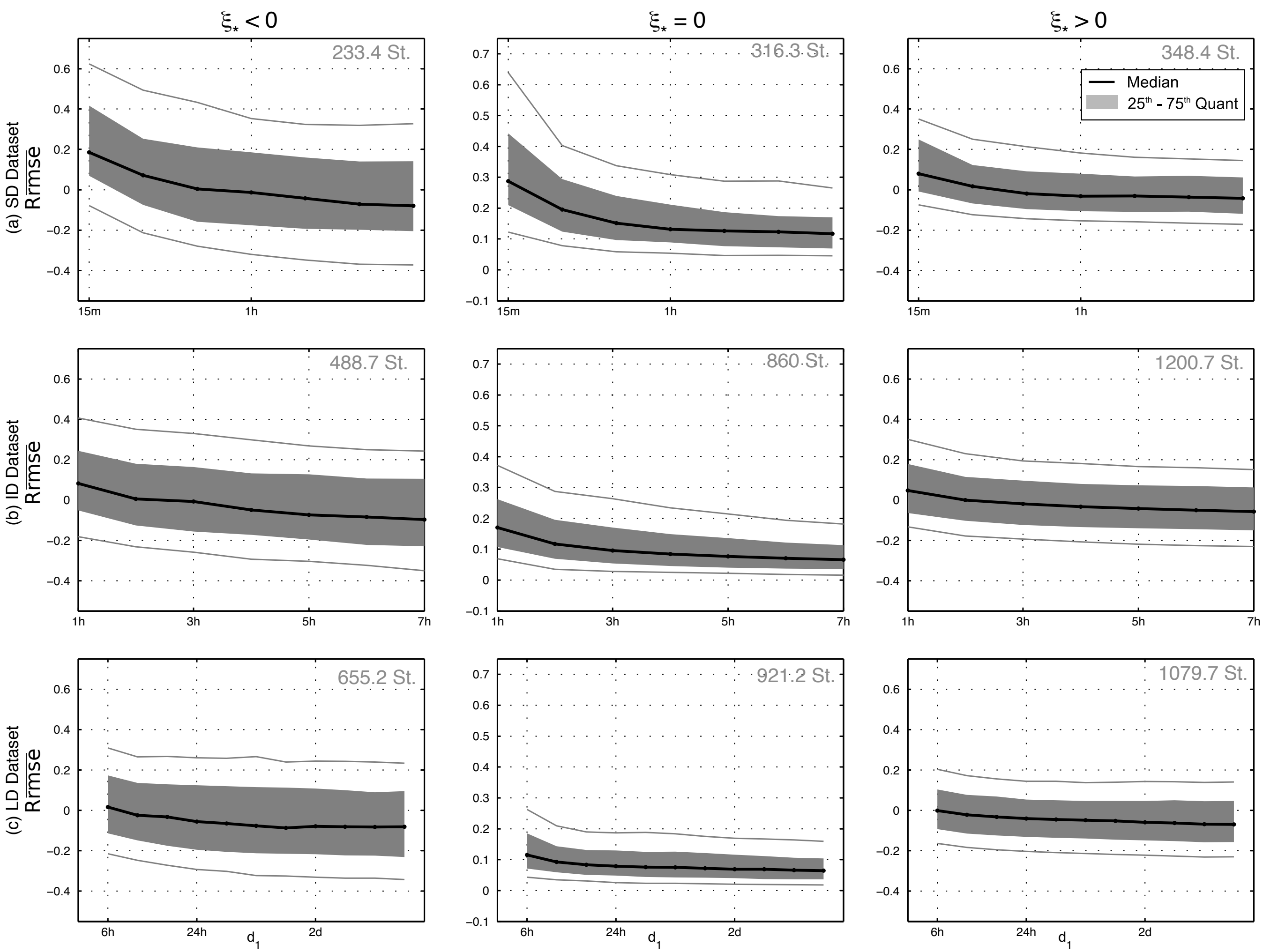

Figure S16. Distribution of the relative total RMSE ratio, $R_{\overline{rmse}}$, for $\xi_* < 0$ (1^st col.), $\xi_* = 0$ (2^nd col.), and $\xi_* > 0$ (3^st col.) for 18-duration scaling intervals in SD, ID, and LD datasets [(a), (b), and (c), respectively].

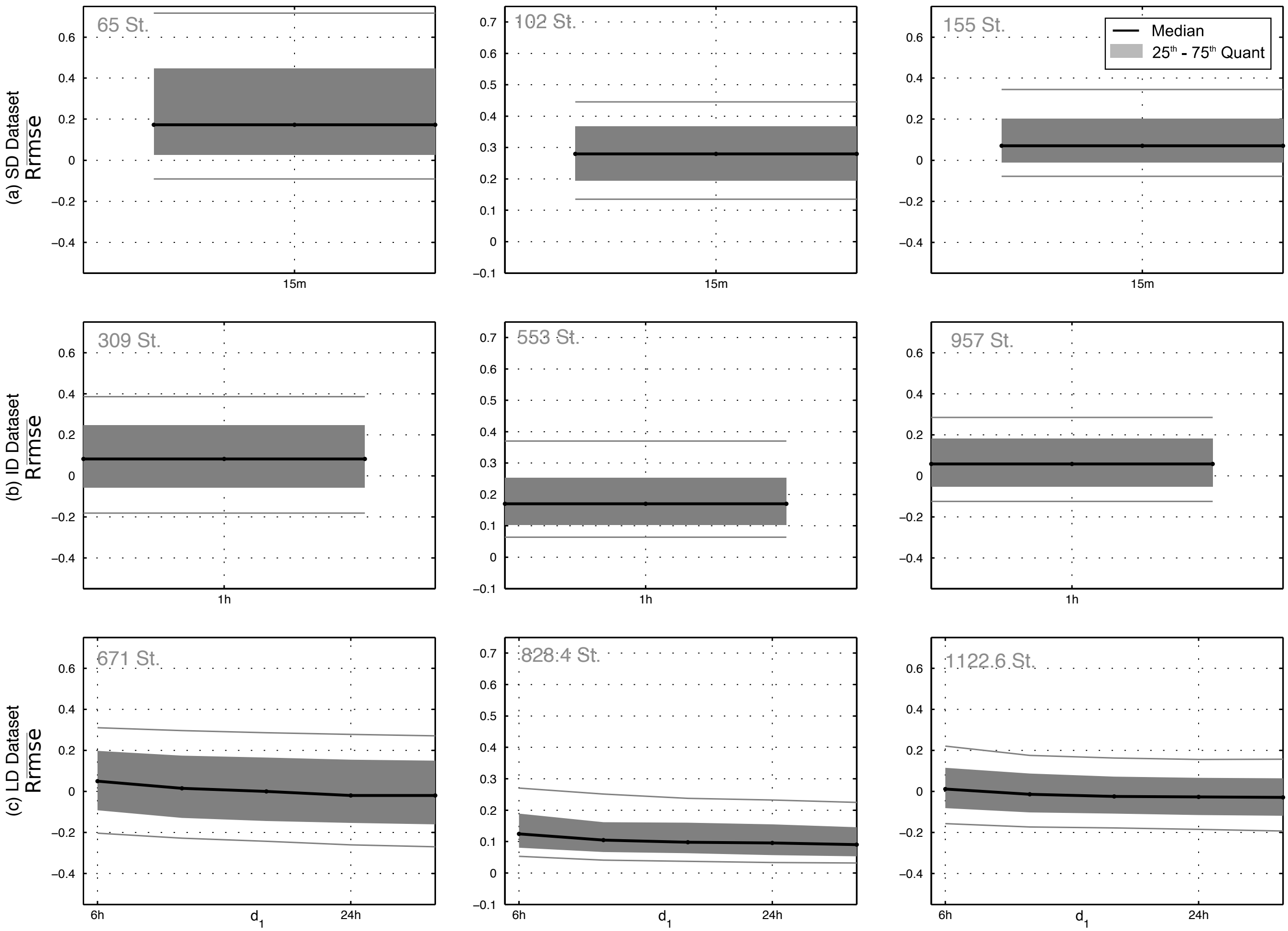

Figure S17. Distribution of the relative total RMSE ratio, $R_{\overline{rmse}}$, for $\xi_* < 0$ (1^st col.), $\xi_* = 0$ (2^nd col.), and $\xi_* > 0$ (3^st col.) for 24-duration scaling intervals in SD, ID, and LD datasets [(a), (b), and (c), respectively].